A New Nonhydrolytic Synthesis of Magnetite Nanocrystallites in the Presence of ω-Functionalized Polystyrene Matrix

Liming Jiang[1], Jungahn Kim[2]

[1]*Department of Polymer Science and Engineering, Zhejiang University, Hangzhou 310027, People's Republic of China*
[2]*Polymer Hybrids Research Center, Korea Institute of Science and Technology, Seoul 130–650, Republic of Korea*

Received 5 January 2005; accepted 26 June 2005
DOI 10.1002/app.23167
Published online in Wiley InterScience (www.interscience.wiley.com).

ABSTRACT: This article describes the synthesis of iron oxide nanocomposites from thermal decomposition of iron(III) acetylacetonate, in organic medium, in the presence of linear ω-functionalized polystyrenes. The nature of the magnetic particles was identified as magnetite (Fe_3O_4), based on X-ray powder diffraction and Raman spectroscopy, while the morphology and particle size of the so-prepared materials were evaluated by TEM technique. The resultant magnetic composites, with average particle sizes below 10 nm, can be easily dissolved in organic solvents, producing stable organosols. Magnetization measurements revealed that the nanocomposites exhibit superparamagnetic behavior at room temperature. © 2006 Wiley Periodicals, Inc. J Appl Polym Sci 101: 186–191, 2006

Key words: thermolysis; iron(III) acetylacetate; ω-functionalized polystyrene; nanocomposite; magnetic property

INTRODUCTION

During the past decade, synthesis of magnetic materials on the nanoscale has been a field of intense study, because of the technological importance and scientific research interest.[1,2] Below a critical size, magnetic nanoparticles become single-domain and exhibit unique phenomena, such as superparamagnetism, quantum tunneling of the magnetization, and unusually large coercivities,[3] providing application potentialities in information storage, controlled drug delivery, and magnetic resonance imaging. However, very different physical properties, especially magnetic behaviors, have been observed with materials having similar grain sizes, but produced distinct methods, and therefore possesses varied microstructures, such as different coatings, size uniformity, and crystallinity.[4] As a consequence, developing synthetic routes to achieve rigorous control of the microstructures of iron oxide nanoparticles is of particular importance, for the applications of these magnetic nanomaterials.

Magnetite (Fe_3O_4) nanoparticles are commonly prepared via coprecipitation of ferrous and ferric ions by a base, in an aqueous solution, or they may be produced by thermal decomposition of alkaline solution of Fe^{3+} chelate in the presence of hydrazine and by sonochemical decomposition of hydrolyzed Fe(II) salt, followed by thermal treatment.[5–7] A variety of functionalized polymers have been used as matrix, for the aqueous preparation of Fe_3O_4-nanocomposites.[8–13] Recently, organic solution-phase decomposition of the iron precursor at high temperatures has been developed for iron oxide nanoparticle synthesis. It has been demonstrated that direct decomposition of $FeCup_3$ (Cup: N-nitrosophenylhydroxylamine) and $Fe(acac)_3$, or decomposition of $Fe(CO)_5$ followed by oxidation,[14–16] can lead to monodisperse oxide nanoparticles. In these procedures, the long-chain aliphatic acid or amine or both is usually the surfactant of choice for oxide nanocrystals. In the present work, we describe a thermolysis method for the preparation of highly crystalline Fe_3O_4 nanoparticles, in which ω-functionalized polystyrenes were first used as a protecting agent, instead of the well-known oleic acid or oleylamine. This method allows the synthesis of magnetic nanocomposites, which contain magnetite, with a maximum content of 37 wt %. The as-prepared composites were characterized by the transmission electron microscopy (TEM), Raman spectrometry, X-ray powder diffraction (XRD), and thermogravimetric analysis (TGA), and their magnetic properties have been investigated by SQUID magnetometry.

EXPERIMENTAL

Chemicals and materials

All chemicals were of reagent grade and used without further purification. Iron(III) acetylacetonate [$Fe(acac)_3$],

Correspondence to: L. Jiang (cejlm@zju.edu.cn).
Contract grant sponsor: National Natural Science Foundation of China; contract grant number: 20274036.
Contract grant sponsor: Korea Foundation for Advanced Studies (KFAS) International Scholar Exchange Fellowship Program (2002–2003).

1,2-hexadecanediol (tech., 90%), phenyl ether, and diphenylmethane were purchased from Aldrich Chemical Co. (USA). Tetrahydrofuran (THF), toluene, and methanol were used as received from J.T. Baker (USA). The polymeric matrices used in this study include ω-sulfonate polystyrene ($PSSO_3H$, M_w 5K), ω-thiolated polystyrene (PSSH, M_w 5K), and ω-carboxylate polystyrene ($PSCO_2H$, M_w 39.4K), which were synthesized by the living anionic polymerization, in this laboratory, and have a narrow molecular weight distribution ($M_w/M_n <$ 1.1 determined by GPC).

Preparation of F_3O_4 nanocomposites

$Fe(acac)_3$ (0.2 mmol) was mixed with 1,2-hexadecanediol (0.1 mmol) and polymer (125 mg) in phenyl ether or diphenyl methane (25 mL) under Argon atmosphere, and then the mixture was heated to reflux for 30 min. The solution was cooled to room temperature, and methanol was added to yield a dark-brown precipitate and left overnight. The precipitate was collected and washed with a large amount of methanol, to remove the remaining solvent. Adding 30 mL of THF to this precipitate, with stirring and separating the insoluble matter, gave a deep-brown solution. The powder product could be obtained by either concentrating the THF solution under vacuum or reprecipitation with methanol.

Characterization of materials

UV–visible absorption spectra were obtained by Hewlett–Packard 8453A Diode Array spectrophotometer. Raman spectra were recorded from 4000 to 200 cm^{-1}, on a Nicolet Almega spectrometer. Powders were sampled on a glass plate, while a frequency double Nd:YAG laser (532 nm, 10 mW) was focused using a Olympus microscope (magnification ×50). The XRD was obtained on a MacScience MXP18 diffractometer, using Cu Kα radiation at wavelength λ = 1.5405 Å. Diffraction patterns were measured in 40 kV and 100 mA, with 1°/min scan speed. The distances between peaks (d) were calculated according to the Bragg's law. A crude estimate of the particle size (D) can be deduced from the Scherrer equation.[17] TEM techniques (Philips CM) were employed to examine the morphology and the microstructure of composite samples. TGA was carried out on a DuPont TGA 2950 in N_2 atmosphere, between room temperature and 600°C, at a heating rate of 10°C/min. Magnetic property of the composites was studied using Physical Properties Measurement System (Model: PPM-9, Quantum Design), at fields ranging from −20 to 20 k Oe, and at temperatures from 5 to 300 K.

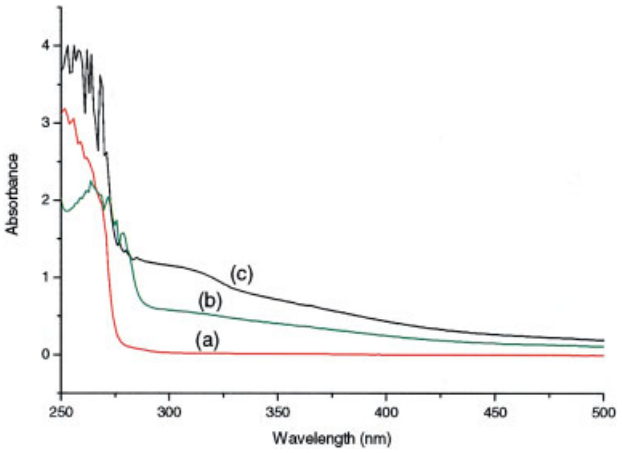

Figure 1 UV–vis spectra of (a) PSSH, (b) sample B7, and (c) sample B6 in THF solution. [Color figure can be viewed in the online issue, which is available at www.interscience.wiley.com.]

RESULTS AND DISCUSSION

Synthesis and characterization

Sun and Zeng[15] reported that a nonhydrolytic route based on the thermal decomposition of iron(III) acetylacetonate, in the presence of oleic acid and oleylamine, led to monodisperse magnetite nanoparticles. Following this precedent, in the present work, we explored the possibility of employing ω-functionalized polystyrenes ($PSSO_3H$, $PSCO_2H$, and PSSH) as rigid matrices, for the synthesis of iron oxide nanocomposites. Although the crosslinked polystyrene resin has been used to make nanomaterials,[8,12,18] there are few reports for the preparation of linear ω-functionalized polymer-stabilized nanoparticles up to date.[19]

As described in the experimental, the thermolysis of $Fe(acac)_3$ was carried out in boiling phenyl ether or diphenlymethane solution, containing both the polymer and 1,2-hexadecanediol. The reaction temperature was 259 and 264°C for both systems, respectively. It should be noted that the precipitation isolated from the reaction mixture consisted of two parts: one could be soluble in THF and another was insoluble. However, both samples exhibited almost the same XRD patterns, with characteristics of magnetite (Fe_3O_4), suggesting that they may be identical in the nature (*vide post*). The amount of THF-insoluble matter varied, depending on reaction conditions. Adding methanol to the THF-soluble fraction gave a deep-brown powder, which could also be dissolved by other suitable solvents, such as toluene, chloroform, and DMF. The as-formed transparent organosols remained stable after 6 months. Figure 1 shows the UV–vis spectra of these samples, with different core sizes, together with that of pure PSSH matrix in THF solution. ω-Functionalized PS was found to absorb below 300 nm; hence,

TABLE I
Comparison of Fe_3O_4-Nanocomposites Synthesized by the High-Temperature Decomposition Route under Different Reaction Conditions[a]

No.	Polymer (MW)	Solvent[b]	% yield[c]	Wt % Fe_3O_4[c]	D_{TEM} (nm)[d]
B1	$PSSO_3H$ (5K)	PE	25	32.59	7–15 (9.1)
B2	$PSSO_3H$ (5K)	DPM	32	6.32	5–15 (8.7)
B3	$PSCO_2H$ (39.4K)	PE	68	17.02	3–12 (6.7)
B4	$PSCO_2H$ (39.4K)	DPM	60	9.77	5–10 (7.6)
B5	PSSH (5K)	PE	94	37.31	3–12 (7.2)
B6	PSSH (5K)	DPM	82	8.33	2–10 (8.1)
B7	PSSH (5K)[e]	PE	86	8.3	2–6 (4.6)

[a] $Fe(acac)_3$, 0.2 mmol (72.8 mg); polymer, 125 mg; solvent, 25 mL; 1,2-hexadecanediol, 0.1 mmol (28.8 mg); refluxed for 30 min under Argon atmosphere.
[b] PE, phenyl ether; DPM, diphenylmethane.
[c] Based on TGA.
[d] Average sizes determined by statistical analysis of the TEM images in parentheses.
[e] PSSH 250 mg, others were the same as in footnote *a*.

the absorption between 300 and 450 nm can be attributed to the iron oxide embedded nanoparticles. In these spectra, broad absorption bands extend to ~450 nm, without distinct peaks, which is similar to that reported for other systems.[9]

Since THF-soluble samples are composed of nanosized oxide cores and polystyrene matrix, the inorganic content was determined by TGA. The yield of nanoparticles was calculated, assuming that $Fe(acac)_3$ is completely converted to Fe_3O_4 (Table I). In all TG curves, rapid weight loss occurred above 350°C, and no further weight loss was observed above 500°C. We suggest that observed weight loss is mainly attributed to burning out of organic phase. As shown in Table I, the decomposition reaction was related with the polymer bearing different groups in terms of the yield. For example, the low conversion of Fe(III) precursor into oxide was observed in the case of $PSSO_3H$. The result implied that $PSSO_3H$ is less effective at the formation of nanoparticles, as well as the particle's stabilization, which may be described to its poor affinity of sulfonic group to the oxide particle surface. Comparatively, PSSH and $PSCO_2H$ are more efficient as a capping agent for iron oxide particles, under present reaction conditions. As for solvent, phenyl ether appears to be in favor of producing high-loaded composites compared with diphenylmethane, although both of them have a nearly same boiling point (see Table I).

A set of comparison experiments were carried out to detect the role of the polymeric matrix in the formation of nanoparticles. The results showed that the same procedure failed to yield the magnetic composites, dissolvable in toluene or THF, only without the presence of ω-functionalized polystyrenes. It was also demonstrated that decreasing the ratio of $Fe(acac)_3$ to polymer in starting reaction feed could produce oxide nanoparticles with a smaller size, as shown in sample B7 in Table I. Consequently, we suspect that the poly-

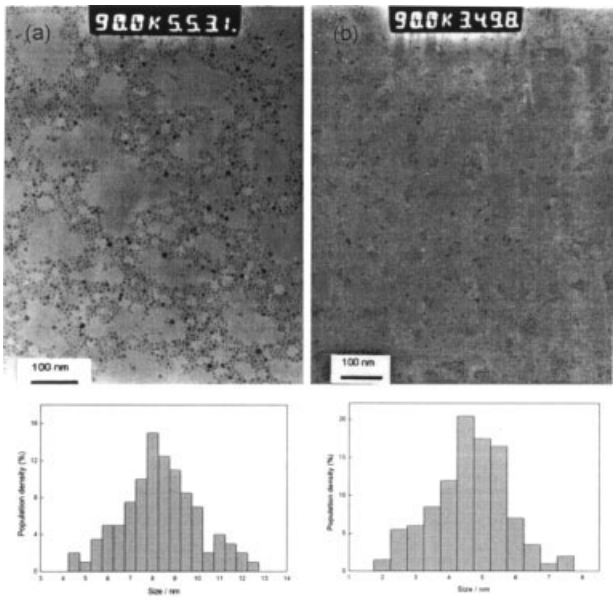

Figure 2 TEM images of samples B6 (a) and B7 (b) in Table I, and corresponding particle size histograms that are obtained by measuring the diameter of 500 particles.

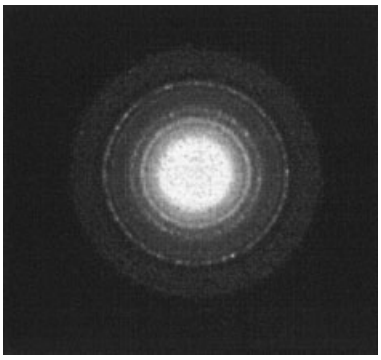

Figure 3 Selected-area electron diffraction pattern of the corresponding magnetite nanocrystals, as shown in Figure 2(a).

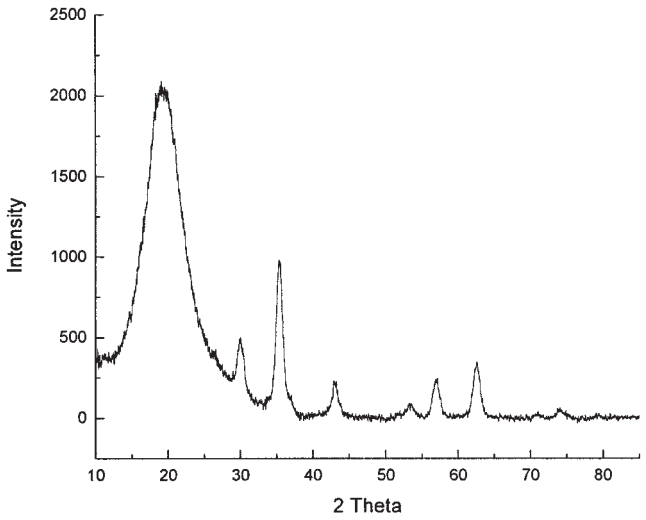

Figure 4 Typical XRD pattern of the synthesized magnetite-composite (sample B6 in Table I).

mer materials would serve as a template to confine the growth of oxide particles, and *in situ* generated nanoparticles were coated with polymer shell. On the other hand, 1,2-hexadecanediol was proved to be an essential component to transform $Fe(acac)_3$ into iron oxide. Although a possible alcohol reduction route has been proposed previously,[15] the exact reaction mechanism was not understood.

TEM was used to examine the particle size and morphology of the nanocomposites. In all cases, the average core sizes were lower than 10 nm (Table I), indicating that the kind of polymer matrix or solvent has no significant effect upon the particle size. Typical TEM images and corresponding histograms of size distribution are depicted in Figure 2. It can be seen that the particles are nearly spherical in shape, and each particle is separated from neighboring particles by its polymer shell. However, the particle profile is not so clear for sample B7 [Fig. 2(b)], which may be described to lower the density of oxide particles in the polymer matrix. The size distributions are located at 6–10 nm and 4–6 nm for samples B6 and B7, respectively. Apparently, the relatively broad size distribution prevents the formation of ordered superlattices, as observed with other systems.[14–16]

Selected area electron diffraction patterns were collected from freshly prepared samples of the nanocomposites. The distinct pattern indicates the single crystal nature of iron oxide nanoparticles in the composites (Fig. 3). The XRD patterns further evidenced their high crystallinity, as shown in Figure 4. For all samples, a broad peak was found at $d \approx 4.7$ Å, which could be attributed to the polymer matrix and other diffraction peaks belonging to the polycrystalline iron oxide phase. The crystallization of nanoparticles at the most intense peak corresponds to the (311) reflection in Fe_3O_4. The average crystallite sizes measured from the Scherrer's equation[17] were fairly in agreement with those estimated by statistical analysis of the TEM images. It can be seen that the *d*-spacing values of the nanocrystallites, prepared from different systems, correspond closely to those of both Fe_3O_4 (magnetite) and γ-Fe_2O_3 (maghemite) (Table II). Thus, Raman spectroscopy was employed to further determine the nature of oxide cores. Figure 5 is a typical Raman spectrum of as-prepared composites, which revealed a characteristic peak at 669 $cm^{-1}$of magnetite. Comparing the spectrum with those of the iron oxides reported[20–22] permitted that the inorganic cores composed mainly of Fe_3O_4.

Magnetic properties

The magnetization of ferromagnetic materials, such as magnetite and maghemite, is very sensitive to the microstructure of a particular sample. If a specimen consists of small particles, its total magnetization decreases with particle size because of increasing dispersion on the exchange integral, and finally reaches the superparamagnetic state when each particle acts as a "spin", with suppressed exchange interaction between the particles.[23] Figure 6 presents magnetization as a

TABLE II
The *d* Values (Å) of Samples Prepared under Different Reaction Conditions via XRD Analysis and Those of γ-Fe_2O_3 and Fe_3O_4 from the JCPDS Database[a]

B1	B2	B3	B4	B5	B6	γ-Fe_2O_3[b]	Fe_3O_4[c]
2.9616	2.9635	2.9760	2.9691	2.9616	2.9694	2.953	2.967
2.5294	2.5272	2.5265	2.5327	2.5283	2.5405	2.5177	2.532
2.0859	2.1072	2.1157	2.0973	2.0933	2.0957	2.0886	2.0993
1.7110	1.7149	1.7135	1.7095	1.7110	1.7170	1.7045	1.7146
1.6165	1.6114	1.6101	1.6114	1.6137	1.6148	1.6073	1.6158
1.4795	1.4833	1.4810	1.4807	1.4890	1.4823	1.4758	1.4845

[a] α-Fe_2O_3 and Fe have distinctively different XRD patterns.
[b] JCPDS card number: 39–1346.
[c] JCPDS card number: 19–629.

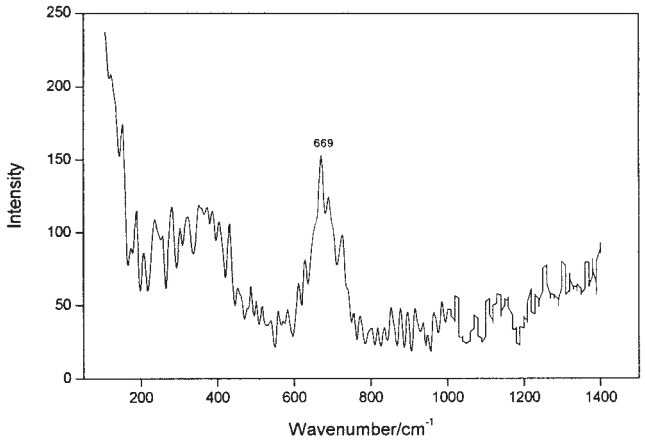

Figure 5 Raman spectrum of the synthesized nanocomposite (sample B6 in Table I).

function of applied magnetic field for the as-prepared nanocomposite (sample B3 in Table I) at room temperature. There is no hysteresis at room temperature, which is consistent with superparamagnetic behavior. For this sample with magnetite loading of ~7%, the saturation magnetization (σ_s) is about 3.5 emu/g at 30 kG. When expressed per gram of magnetite in the nanocomposites, σ_s equals ~50 emu/g of Fe_3O_4. Apparently, the larger distribution and smaller size of particles decreases σ_s considerably because of relaxation effects of spins on the surface atoms.[24]

The temperature dependence of the magnetization was measured using zero-field cooling (ZFC) and field cooling (FC) procedures, in an applied magnetic field of 100 Oe, between 5 and 300 K (Fig. 7). Above 50 K, the magnetization decreases with increasing temperature in both the ZFC and the FC case. At lower temperatures, the magnetization increases monotonically

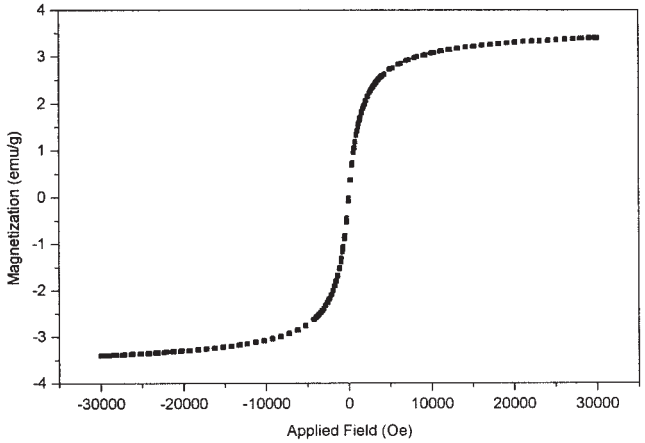

Figure 6 Magnetization versus applied magnetic field for $PSCO_2H$-coated magnetite nanocomposite (sample B3 in Table I).

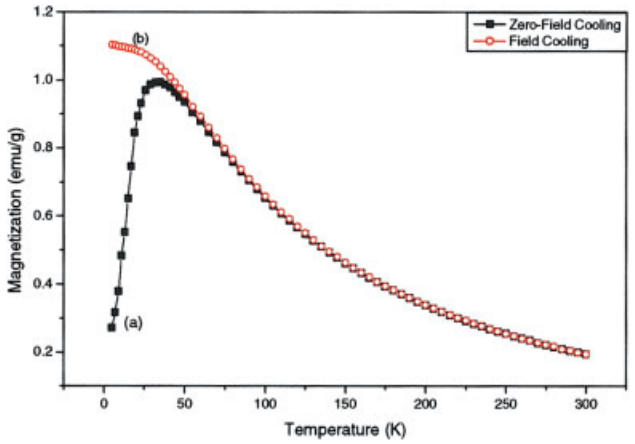

Figure 7 Magnetization versus temperature for $PSCO_2H$-coated magnetite nanocomposite (sample B3 in Table I) at H = 100 Oe. (a) ZFC; (b) FC. [Color figure can be viewed in the online issue, which is available at www.interscience.wiley.com.]

with decreasing temperature for the FC case, whereas the ZFC magnetization passes through a maximum at ~40 K, which can be associated with the blocking temperature.[25]

CONCLUSIONS

In this study, we developed a new preparative approach for magnetite nanocrystallites, based on the thermal decomposition of $Fe(acac)_3$ in the presence of ω-functionalized polystyrenes. The synthetic procedures allow Fe_3O_4-nanocomposites with a high loading (up to 37%) to be obtained. By changing the ratio of iron precursor to polymer matrices, the particle size could be altered in the range of 4–10 nm. The magnetic measurements revealed that the nanocomposites are superparamagnetic and showed no remanence or coercivity at room temperature. Owing to their easy availability and special stability in organosol state, the resultant hybrid materials would be expected to have some potential applications.

The author thanks Mr. Soochul Kim for his assistance with TEM measurements and Changwoo Lee for the XRD and TGA measurements. The main studies were completed at Prof. Jungahn Kim's laboratory, Korea Institute of Science and Technology (KIST).

References

1. Alivisatos, A. P. Science 1996, 271, 933.
2. Schmid, G. Clusters and Colloids; VCH: New York, 1994.
3. Dormann, J. L.; Fiorani, D. Magnetic Properties of Fine Particles; North-Holland: New York, 1991.
4. Morales, M. P.; Veintemillas-Verdaguer, S.; Montero, M. I.; Serna, C. J. Chem Mater 1999, 11, 3058.
5. Fried, G. T.; Markovich, G. S. Adv Mater 2001, 13, 1158.

6. Sapieszko, R. S.; Matijevic, E. J Colloid Interface Sci 1980, 74, 405.
7. Vijayakumar, R.; Koltypin, Y.; Felner, I.; Gedanken, A. Mater Sci Eng A 2000, 286, 101.
8. Ziolo, R. F.; Giannelis, E. P.; Weinstein, B. A.; O'Horo, M. P.; Ganguly, B. N.; Mehrotra, V.; Russell, M. W.; Huffman, D. R. Science 1992, 257, 219.
9. Sohn, B. H.; Cohen, R. E. Chem Mater 1997, 9, 264.
10. Kumar, R. V.; Koltypin, Y.; Cohen, Y. S.; Cohen, Y.; Aurbach, D.; Palchik, O.; Felner, I.; Gedanken, A. J Mater Chem 2000, 10, 1125.
11. Lee, J.; Isobe, T.; Senna, M. J Colloid Interface Sci 1996, 177, 490.
12. Ding, X.; Sun, Z.; Zhang, W.; Peng, Y.; Chan, A. S. C.; Li, P. Colloid Polym Sci 2000, 278, 459.
13. Breulmann, M.; Cölfen, H. Adv Mater 1998, 10, 237.
14. Rockenberger, J.; Scher, E. C.; Alivisatos, P. J Am Chem Soc 1999, 121, 11595.
15. Sun, S.; Zeng, H. J Am Chem Soc 2002, 124, 8204.
16. Hyeon, T.; Lee, S. S.; Park, J.; Chung, Y.; Na, H. B. J Am Chem Soc 2001, 123, 12798.
17. Klug, H.; Alexander, L. X-Ray Diffraction Procedures for Polycrystalline and Amorphous Materials; Wiley: New York, 1962; p 491.
18. Burke, N. A. D.; Stver, H. D. H.; Dawson, F. P. Chem Mater 2002, 14, 4762.
19. Kim, J.; Jim, S. S.; Kim, K. H.; Jin, Y. H.; Hong, S. M.; Hwang, S. S.; Cho, B.-G.; Shin, D. Y.; Im, S. S. Polymer 2004, 45, 3527.
20. de Faria, D. L. A.; Silva, S. V.; de Oliveira. M. T. J Raman Spectrosc 1997, 28, 873.
21. Ohtsuka, T.; Kubo, K.; Sato, N. Corrosion 1986, 42, 476.
22. Thierry, D.; Persson, D.; Leygraf, C.; Boucherit, N.; Hugotle Goff, A. Corros Sci 1991, 32, 273.
23. Elliott, S. R. Physics of Amorphous Materials; Longman: London/New York, 1984; p 350.
24. Sudakar, C.; Subbanna, G. N.; Kutty, T. R. N. J Mater Chem 2002, 12, 107.
25. Vassiliou, J. K.; Mehrotra, V.; Russell, M. W.; Giannelis, E. P.; McMichael, R. D.; Shull, R. D.; Ziolo, R. F. J Appl Phys 1993, 73, 5109.